Acta Oceanol. Sin., 2014, Vol. 33, No. 12, P. 107–117
DOI: 10.1007/s13131-014-0580-9
http://www.hyxb.org.cn
E-mail: hyxbe@263.net

Analyses on the tectonic thermal evolution and influence factors in the deep-water Qiongdongnan Basin

WANG Zhenfeng[1], SHI Xiaobin[2]*, YANG Jun[2,3], HUANG Baojia[1], SUN Zhen[2], WANG Yahui[1], JIANG Haiyan[2], YU Chuanhai[2,3], YANG Xiaoqiu[2]

[1] Zhanjiang Branch of China National Offshore Oil Corporation (CNOOC) Limited, Zhanjiang 524057, China
[2] Key Laboratory of Marginal Sea Geology, South China Sea Institute of Oceanology, Chinese Academy of Sciences, Guangzhou 510301, China
[3] University of Chinese Academy of Sciences, Beijing 100039, China

Received 20 June 2014; accepted 29 September 2014

Abstract

To reveal the tectonic thermal evolution and influence factors on the present heat flow distribution, based on 154 heat flow data, the present heat flow distribution features of the main tectonic units are first analyzed in detail, then the tectonic thermal evolution histories of 20 profiles are reestablished crossing the main deep-water sags with a structural, thermal and sedimentary coupled numerical model. On the basis of the present geothermal features, the Qiongdongnan Basin could be divided into three regions: the northern shelf and upper slope region with a heat flow of 50–70 mW/m^2, most of the central depression zone of 70–85 mW/m^2, and a NE trending high heat flow zone of 85–105 mW/m^2 lying in the eastern basin. Numerical modeling shows that during the syn-rift phase, the heat flow increases generally with time, and is higher in basement high area than in its adjacent sags. At the end of the syn-rift phase, the heat flow in the deep-water sags was in a range of 60–85 mW/m^2, while in the basement high area, it was in a range of 75–100 mW/m^2. During the post-rift phase, the heat flow decreased gradually, and tended to be more uniform in the basement highs and sags. However, an extensive magmatism, which equivalently happened at around 5 Ma, has greatly increased the heat flow values, and the relict heat still contributes about 10–25 mW/m^2 to the present surface heat flow in the central depression zone and the southern uplift zone. Further analyses suggested that the present high heat flow in the deep-water Qiongdongnan Basin is a combined result of the thermal anomaly in the upper mantle, highly thinning of the lithosphere, and the recent extensive magmatism. Other secondary factors might have affected the heat flow distribution features in some local regions. These factors include basement and seafloor topography, sediment heat generation, thermal blanketing, local magmatic injecting and hydrothermal activities related to faulting and overpressure.

Key words: northern continental margin, South China Sea, surface heat flow, magmatism

Citation: Wang Zhenfeng, Shi Xiaobin, Yang Jun, Huang Baojia, Sun Zhen, Wang Yahui, Jiang Haiyan, Yu Chuanhai, Yang Xiaoqiu. 2014. Analyses on the tectonic thermal evolution and influence factors in the deep-water Qiongdongnan Basin. Acta Oceanologica Sinica, 33(12): 107–117, doi: 10.1007/s13131-014-0580-9

1 Introduction

The significant breakthroughs (Pang et al., 2006; Wang et al., 2011) achieved recently in the deep-water oil and gas exploration on the northern continental margin of the South China Sea, suggest strongly that these deep-water areas are of great potentials of hydrocarbon resources. The studies on the thermal regime of these deep-water areas are helpful not only to understand their tectonic evolution and geodynamic processes, but also to obtain a reliable hydrocarbon resource evaluation, thus to reduce the exploration cost and risk (White et al., 2003; Zhang et al., 2010). Though the thermal regime of the Qiongdongnan Basin has been widely studied (e.g., He et al., 2001; Zhang and Wang, 2000; Shi et al., 2003; Yuan et al., 2009; Mi et al., 2009; Song et al., 2011; Shan et al., 2011), these studies were based on the heat flows located on the northern shelf, and could not well constrain the thermal regime in the deep-water region. Furthermore, the employed numerical models could not deal with the sedimentary thermal effect due to their thermal blanketing. It is now believed that the sedimentary effect on the lithosphere and basin thermal processes could not be ignored (Rupke et al., 2008), particularly in a basin covered by very thick sediment. Recently, with the deep-water hydrocarbon exploration, a new set of valuable drill-derived and seafloor probe heat flow data has been obtained in the Qiongdongnan Basin (Xu et al., 2006)①. In this contribution, we first analyzed the present heat flow distribution characteristics of the deep-water Qiongdongnan Basin, then employed a structural, thermal and sedimentary coupled numerical model to rebuild the tectonic thermal evolution of the deep-water area, finally discussed on the influence factors on the thermal evolution and heat flow distribution.

Foundation item: the National Science and Technology Major Programs of China under contract No. 2011ZX05025-002-01; the National Natural Science Foundation of China under contract Nos 41176050 and 41376059.
*Corresponding author, E-mail: xbshi@scsio.ac.cn
①Shi Xiaobin, Wang Zhenfeng, Jiang Haiyan, et al. 2015. Vertical variations of geothermal parameters in rifted basin, and analyses on heat flow distribution features of the Qiongdongnan Basin. Chinese Journal of Geophysics

2 Geological backgrounds

The NE-running Qiongdongnan Basin, lying between the Hainan Island and the Xisha block, is generally a basin (Fig. 1), is jointed to the west with the Yinggehai Basin, and connected to the east with the northwestern subbasin of the South China Sea through the Xisha Trough. From the north to the south, the basin consists of the northern depression zone, the northern uplift zone, the central depression zone and the southern uplift zone. The northern depression zone could be further divided into the Yabei, Songxi, and Songdong sags from the west to the east, while the central depression zone consists of the Yanan, Ledong, Lingshui, Beijiao, Songnan, Baodao and Changchang sags (Fig. 1). Developed on the pre-Cenozoic basement, the highly rifted basin underwent a syn-rift phase during the Palaeogene, and a Neogene post-rift phase (Gong et al., 1997; Zhong et al., 2004; Wang et al., 2011). As a result, it is of a two-layer structure vertically with a syn-rift lower layer of discrete grabens and half grabens, and a post-rift upper layer of saucer-like downwarps. The Cenozoic in the west is much thicker than that in the east, with a maximum thickness larger than 10 km. Owing to the thick sediment, its initial rifting time is not yet clear. Generally its rifting is assumed to start in the Eocene, and end at around 21 Ma (T60). During the syn-rift phase, the basin accumulated the Eocene, the Early Oligocene Yacheng Formation and the Late Oligocene Lingshui Formation. During the post-rift phase, the faulting became very weak (e.g., Li et al., 2011; Xie et al., 2007; Li and Zhu, 2005), and it accumulated the Early Miocene Sanya Formation, the Middle Miocene Meishan Formation, the Late Miocene Huangliu Formation, the Pliocene Yinggehai Formation, and the Quaternary Ledong Formation. The Xisha Trough is a Cenozoic rifted basin (He, 1980) with a similar tectonic evolution to the Qiongdongnan Basin. The Cenozoic sediment thickness in the trough is about 2–6 km (Yao et al., 1994).

According to the crustal thickness derived from gravity data and seismic data, the Moho depth is about 15–17 km in the Xisha Trough (Qiu et al., 2001), and becomes deeper westward to about 24 km at the Songnan low uplift, then gets shallower westward again to about 22 km in the Lingshui–Ledong sags (Su et al., 2004; Zhang et al., 2007; Zhang et al., 2009; Qin et al., 2011). The thinnest crust, lying in the Xisha Trough, the Changchang sag and the Ledong sag, might be thinner than 10 km, suggesting that the crust in the deep-water Qiongdongnan Basin and the Xisha Trough has been highly stretched and thinned (Zhang et al., 2007). On the basis of seismic reflection profiles and drill samples, extensive post-rift magmatic injections could be identified in the Xisha Trough and Qiongdongnan Basin (e.g., Li et al., 1998).

3 Heat flow distribution features

3.1 *Heat flow data*

Heat flow data are essential for understanding the thermal regime of the study area, and examining the reliability of the geothermal numerical modeling. A data set of 154 heat flows was used in this study, 44 of which were calculated from drill data (hereafter referred to drill heat flow), the rest were obtained by measuring directly with a heat flow probe (hereafter referred to probe heat flow). These probe heat flows include a heat flow section across the Xisha Trough observed jointly by China and USA scientists in the 1980s (Nissen et al., 1995), and

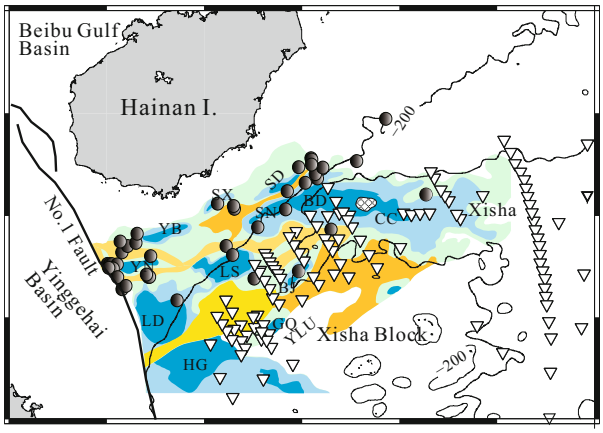

Fig.1. Simplified tectonic framework of the Qiongdongnan Basin. The blue areas show the sags, and the yellow and orange areas show the uplift or the basement high areas. The solid circles show the locations of the drill-derived heat flow stations, and the open triangles are the seafloor probe heat flow stations. YN is short for Yanan sag, YB Yabei sag, SX Songxi sag, SD Songdong sag, SN Songnan sag, BD Baodao sag, CC Changchang sag, LD Ledong sag, LS Lingshui sag, BJ Beijiao sag, HG Huaguang sag, GQ Ganquan sag, YLU Yongle uplift, and Xisha Xisha Trough. The water depth is meter.

those probe heat flow data obtained during the nature gas hydrate investigations in the deep-water Qiongdongnan Basin (e.g., Xu et al., 2006), most of which are still unpublished. The 44 drill heat flows, including four deep-water heat flows, were obtained recently by analyzing oil-gas drill's temperature and logging data. Besides the 20 heat flows of Shi et al.①, the rest 24 drill heat flows are listed in Table 1. The detailed methods of data processing were given in Xu et al. (2006) and Shi et al.①. Since most of these drill heat flows are located on the shelf, and the probe heat flow stations lies in the area where the water depth is larger than 1 000 m, the probe and drill heat flows are highly complementary with each other (Fig. 1). Though due to the different contributions of a sediment heat generation and a thermal blanketing, there are some difference between the probe heat flow and the drill heat flow at a same station, since the drill depth is generally smaller than 4 000 m, our calculations show that the difference is generally lower than 3 mW/m^2. Therefore, they could be analyzed together to uncover the whole heat flow distribution features.

3.2 *Geothermal features of different tectonic units*

Figure 2 is the heat flow distribution trend of the Qiongdongnan Basin based on these heat flow data. The geothermal features of different tectonic units are summarized below.

The heat flow in the northern depression zone is generally lower than 65 mW/m^2. In the eastern depression, the geothermal gradient and heat flow in the Songdong sag are about 40°C/km and (62±10) mW/m^2, respectively. In the central depression, the limited data in the Songxi sag show that its thermal gradient and heat flow are 27°C/km and (50±6) mW/m^2. In the western depression, the average thermal gradient and heat flow in the Yabei sag is 35°C/km and (57±6) mW/m^2, respectively.

Table 1. Drill heat flows in the Qiongdongnan Basin

No.	Drill	Water depth/m	Depth range/mbsf	Average thermal gradient/ °C·km^{-1}	Thermal conductivity /W·m^{-1}·K^{-1}	Heat flow /mW·m^{-2}	Type of temperature data
1	BD1	237.5	2 005	40±5	1.54	61±8	FMT
2	BD2	201.0	4 906	36±3	1.89	69±6	MDT
3	BD3	188.0	3 909	39±4	1.81	71±7	WWL
4	BD4	187.2	2 990	40±5	1.67	67±8	WWL
5	BD5	146.0	1 479	40±7	1.46	58±10	MDT
6	BD6	164.2	1 711	41±6	1.50[1)]	62±9	WWL
7	LS1	167.0	2 923	39±3	1.54	60±5	FMT
8	LS2	189.0	4 318	34±3	1.83	62±6	WWL
9	ST1	147.0	1 990	40±5	1.50	63±8	MDT
10	ST2	171.7	3 891	37±3	1.70[1)]	63±5	MDT
11	ST3	98.0	3 407	27±3	1.87	50±6	BHT
12	YA1	89.3	3 601	43±3	1.69	73±5	BHT,DST
13	YA2	89.0	3 990	40±3	1.69	68±5	BHT,DST
14	YA3	92.0	3 783	41±2	1.68	69±3	BHT,DST
15	YA4	90.8	3 784	41±3	1.71	70±5	BHT,DST
16	YA5	93.4	3 682	38±3	1.70[1)]	66±5	WWL
17	YA6	103.5	4 014	33±3	1.66	55±5	WWL
18	YA7	113.2	5 114	36±3	1.76[1)]	63±5	BHT
19	YA8	106.3	3 506	40±3	1.81[1)]	73±5	BHT
20	YA9	106.7	5 505	41±3	1.90	78±6	BHT
21	YA10	84.9	3 141	40±4	1.75	70±7	BHT
22	YA11	88.1	3 788	35±4	1.64	57±6	BHT
23	YA12	81.7	4 209	35±4	1.64[1)]	67±6	oil test
24	Y1	109.3	2 465	37±4	1.44[1)]	53±6	oil test

Notes: The thermal conductivity was given by the closed drill in the same tectonic unit. WWL is wire-line well log.

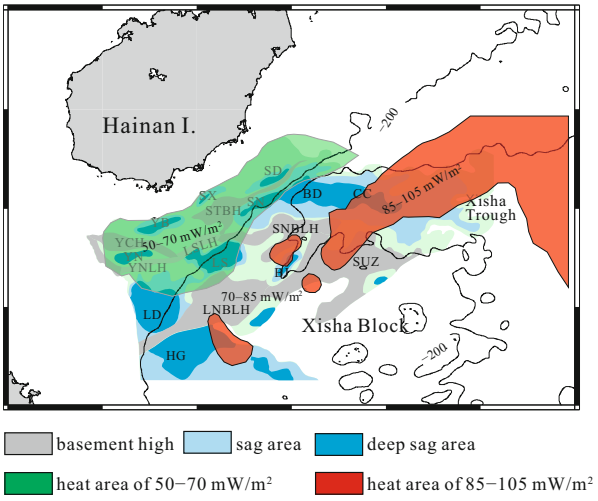

Fig.2. Simplified heat flow trend map of the Qiongdongnan Basin. LNBL is short for Lingnan basement low high, SUZ southern uplift zone, YNLH Yanan low high, LSLH Lingshui low high, SNBLH Songnan basement low high, YCH Yacheng high, and STBG Songtao basement high. Others are the same as Fig. 1.

The heat flow in the northern uplift zone, which lies on the shelf, is generally lower than 70 mW/m^2. The thermal gradient and the heat flow in the western Songtao basement high are 36°C/km, and (52±6) mW/m^2, respectively. The heat flow increases eastward along the Songtao basement high to (63±5) mW/m^2 with a thermal gradient of 37°C/km. In the Yacheng high, the average thermal gradient and the heat flow are about 35°C/km and (60±6) mW/m^2, respectively. In the western slope of the Yanan sag and the Yaxi low basement high, where lies the famous Ya13 great gas field, the thermal gradient ranges from 38°C/km to 43°C/km, and the average heat flow is as high as 68 mW/m^2, indicating a higher thermal background. In the Yanan low basement high and the northern slope of the Ledong sag, the geothermal gradient and the heat flow are 36–41°C/km and 61–78 mW/m^2, respectively, also suggesting a very high geothermal background.

The heat flow in the central depression zone is higher than the northern depression zone. In most of the depression, the heat flow is higher than 70 mW/m^2, and there is a high heat flow zone (>85 mW/m^2) in the eastern basin. There are very few heat flow data in the Ledong sag. However, the data in its adjacent area suggest that the thermal gradient and the heat flow in the sag might be in ranges of 36–41°C/km and 65–75 mW/m^2, respectively. In the southern Ledong sag and the Lingnan low basement high, the heat flow is higher, and in a range of 69–79 mW/m^2 with an average of 74 mW/m^2. In the joint region of the northeastern Huaguang sag, Ganquan sag, Lingnan basement low high and the Yongle uplift, there lies a local high heat flow region of 80–120 mW/m^2. The heat flow in the Ganquan sag is in a range of 68–80 mW/m^2 with an average of 76 mW/m^2. The heat flow of the Lingshui sag is mainly in a range of 60–75 mW/m^2, while in its eastern part, the heat flow is slightly higher and ranges mainly from 70 to 80 mW/m^2 with an average of

75 mW/m^2, and locally higher than 85 mW/m^2. The heat flow in the Beijiao sag and the Beijiao basement high is in a range of 65–95 mW/m^2 with an average of 80 mW/m^2. The heat flow in the Songnan low basement high is 72–83 mW/m^2 with an average of 80 mW/m^2, and some heat flow are higher than 94 mW/m^2. The heat flow on the shelf area of the Songnan sag and the Baodao sag is generally lower than 70 mW/m^2. In the shelf joint area of the Songdong sag, the Songtao basement high and the Baodao sag, the heat flow is in a range of 58–71 mW/m^2, and the thermal gradient is 37–41°C/km with an average of 40°C/km. Toward the deep-water center, the heat flow is in a range of 73–83 mW/m^2 with an average of 77 mW/m^2, higher obviously than the heat flow in the shelf area. In the joint area of the Beijiao high, the Songnan low high and the Baodao-Changchang sag, the heat flow becomes even much higher. This joint area, together with the central Changchang sag and the northern slope of the Xisha Trough, forms a high heat flow zone (>85 mW/m^2). The heat flow of the Changchang sag is in a range of 75–112 mW/m^2, with an average of 95 mW/m^2. Toward to the southern slope of the Changchang sag and the Yongle area, the heat flow decreases to 70–75 mW/m^2. However, in those regions where have developed locally magmatic intrusions since about 5 Ma, the heat flow might be higher than 70–75 mW/m^2.

As a whole, based on the present geothermal features, the Qiongdongnan Basin could be divided into three regions: the northern shelf and upper slope region with a heat flow of 50–70 mW/m^2, most of the central depression zone of 70–85 mW/m^2, and a NE trending high heat flow zone of 85–105 mW/m^2 lying in the eastern basin. This high heat flow zone might be connected with the high heat flow zone in the northern marginal lower slope (Shi et al., 2003) and the high heat flow area of the northwest subbasin of the South China Sea. The heat flow value in the deep-water Qiongdongnan Basin is similar to the northern slope region of the South China Sea.

4 Tectonic thermal evolution of deep-water area

4.1 *Numerical model*

Since sedimentation might have greatly affected the thermal evolution of the lithosphere and the basin (e.g., Rupke et al., 2008), we improved our earlier numerical model (Shi et al., 2008) by coupling the lithospheric stretching deformation and thermal diffusion with sedimentation. The upper boundary condition of the model was set to be a seafloor temperature, and the lower one was assigned the temperature determined on the results of Rayleigh wave tomography (Tang and Zheng, 2013). The average radiogenic heat production rate of the Cenozoic was set to be 1.34 μW/m^3[①]. The palaeo-bathymetry was determined based on the palaeo-geomorphy and sedimentary facies data (Zhu et al., 2007). Since the tectonic subsidence history of the Qiongdongnan Basin has been interfered and cannot constrain its real rifting history[②], the stretching factor was determined based on the crustal thickness variation (McKenzie, 1978) assuming a pre-rift crustal thickness of 32 km. The gravity-derived Moho depth (Zhang et al., 2007) was used for calculating the present crustal thickness.

4.2 *Results*

We have totally calculated 20 profiles trending in NW across these deep-water sags (Fig. 3). In order to obtain a reliable result, we tried to match the calculated present heat flows with the observed heat flow, and to judge the reliabilities by comparing the observed drill's Vitrinite reflectance (R_o, %) and temperature data with the calculated results. Figures 4–7 are the present temperature fields and heat flow histories along Profiles Pm07 and Pm20, respectively. Figure 8 shows heat flow histories of those representative points in different sags (Fig. 3). Generally, the calculated results could well match with the observed temperature, the heat flow and R_o data (e.g., Figs 4–7). However, since these observed data might have been disturbed by some local factors such as hydrothermal activities and overpressure, and the calculated sedimentary thermophysical properties of our numerical model could not be totally the same as the real ones, it was hard to match all these observed data at the same time. For example, in the Ledong sag, though the predicted temperature and heat flow match the observed quite well, the predicted R_o data are generally 0.2–0.4 higher than the observed ones (e.g., Drill YA13), particularly for those R_o samples buried larger than 3 500 m. The lower observed R_o might be the result of overpressure suppression. The overpressure is a widespread phenomenon below a depth of 3 000–4 000 m in the western Qiongdongnan Basin. In the Lingshui, Songnan, Beijiao and Baodao sags, some predicted temperatures are 10–20°C lower than the observed ones. The predicted temperature of Drill LS1 at 3 100 m was 138°C, about 10°C lower than the observed one. The predicted temperature of Drill YL1 at 4 598 m (including the water depth) was 135°C, about 16°C lower than the observed. Some local observed heat flows, which might be affected by some local factors, could not be well matched too.

The results (Figs 4–8) show that during the syn-rift phase, the

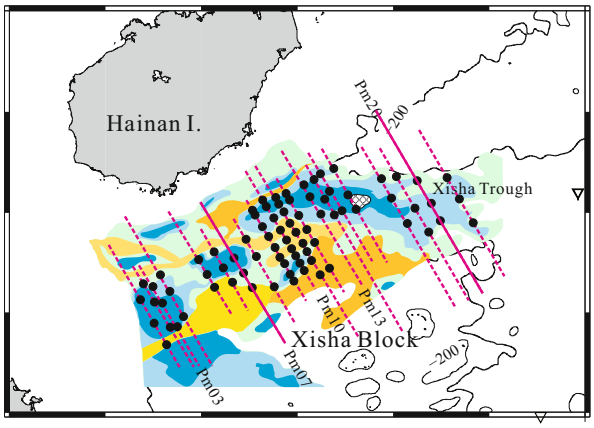

Fig.3. Locations of the calculated profiles and representative points. The solid and dashed lines show the locations of the calculated profiles, and heat flow histories and temperature fields of the solid ones are given below. The profiles are numbered from the west to the east, and the solid circles overlapped these profiles are the representative points, whose heat flow histories are shown in Fig. 5.

[②] Yang Jun, Shi Xiaobin, Wang Zhenfeng, et al. 2015. Causes analyses on syn-rift subsidence deficit and post-rift rapid subsidence in Qiongdongnan Basin. Marine Geology & Quaternary Geology

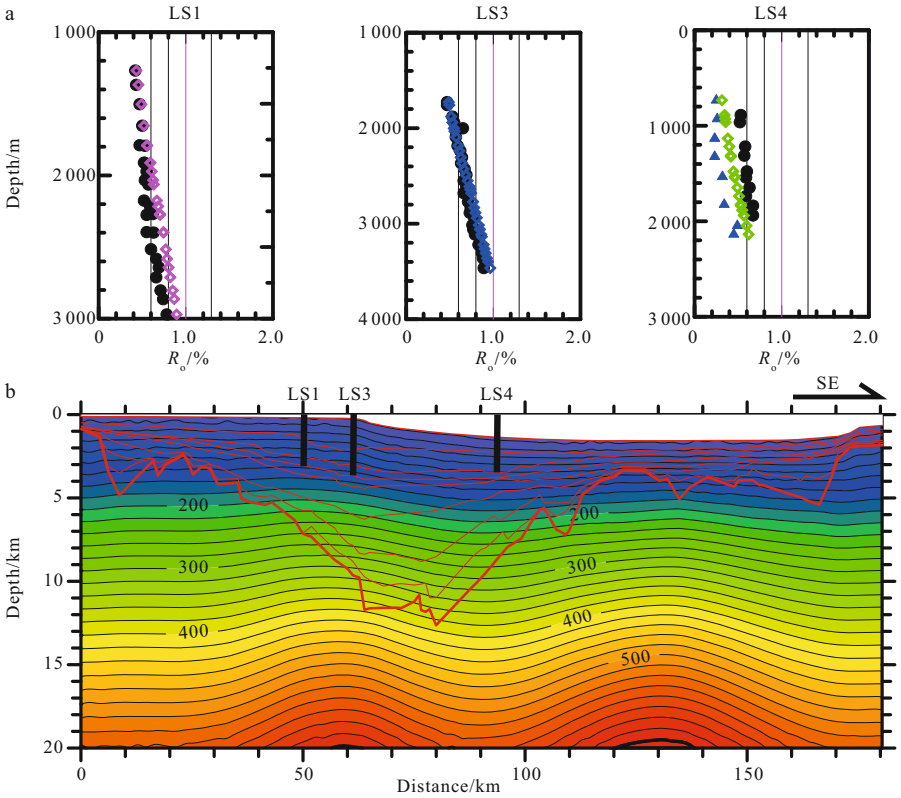

Fig.4. Present temperature field of Pm07 with three drills' observed and calculated R_o-depth data. a. The observed R_o data are shown as solid circles or solid triangles, the calculated R_o are shown as open diamonds. The R_o data depth is the depth below seafloor. b. The red solid lines show the basin basement and the layer interfaces, and the values overlapping the isotherms are the temperatures (°C).

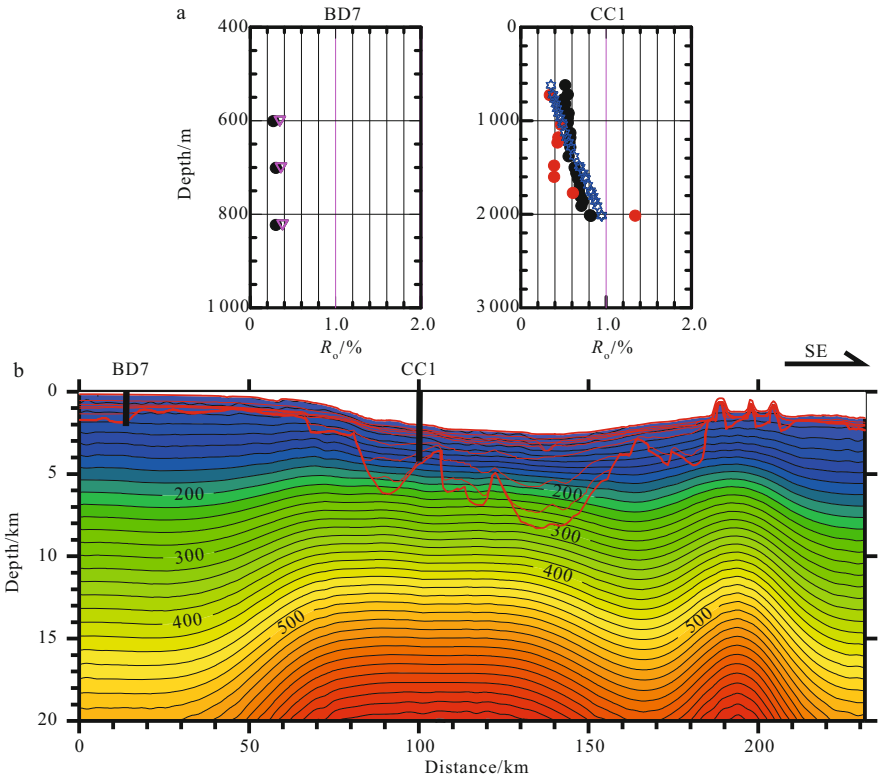

Fig.5. Present temperature field of Pm20 with two drills' observed and calculated R_o-depth data. The observed and calculated R_o data are shown as solid circles and open triangles, respectively. Refer Fig. 4 for other details.

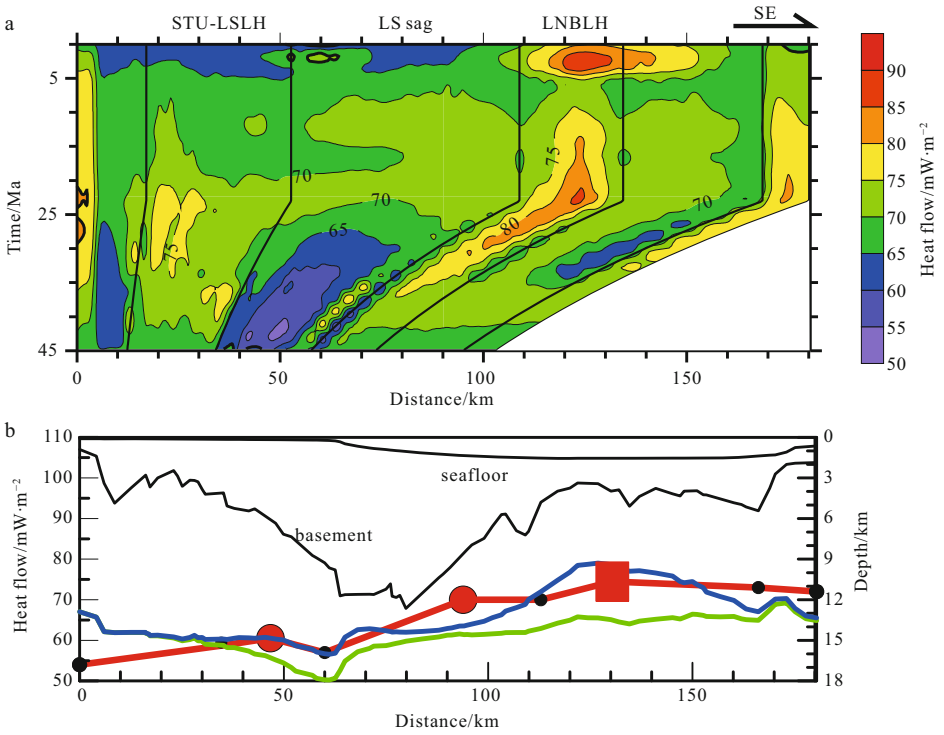

Fig.6. Heat flow evolution (a) and present heat flow variation (b) along Pm07. a. 45 Ma is the initial rifting time. b. The two black lines show the seafloor and the basement, respectively. Red line together with the small black circles show the present heat flow variation obtained from the heat flow distribution (Fig. 2). The red solid circles delegate the heat flow of Drills LS3 and LS4, and the red square shows the observed probe heat flow. The green line shows the predicted present heat flow when there was no recent thermal event, while the blue line is the predicted present heat flow affected by the recent thermal event.

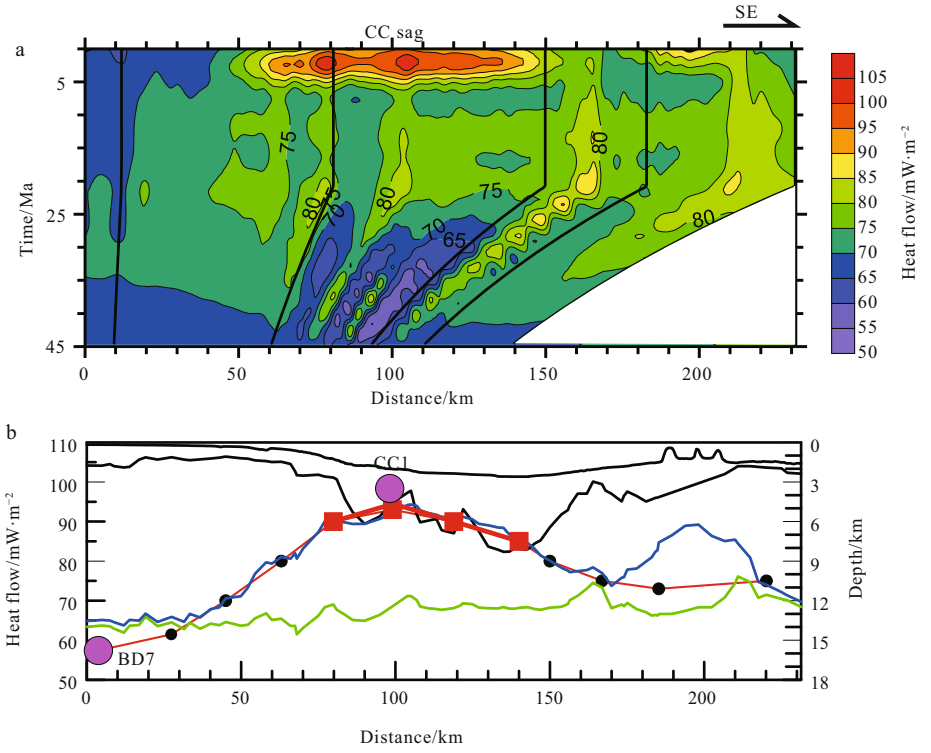

Fig.7. Heat flow evolution (a) and present heat flow variation (b) along Pm20. The red solid circles show the heat flow of Drills BD7 and CC1. Refer to Fig. 6 for other details.

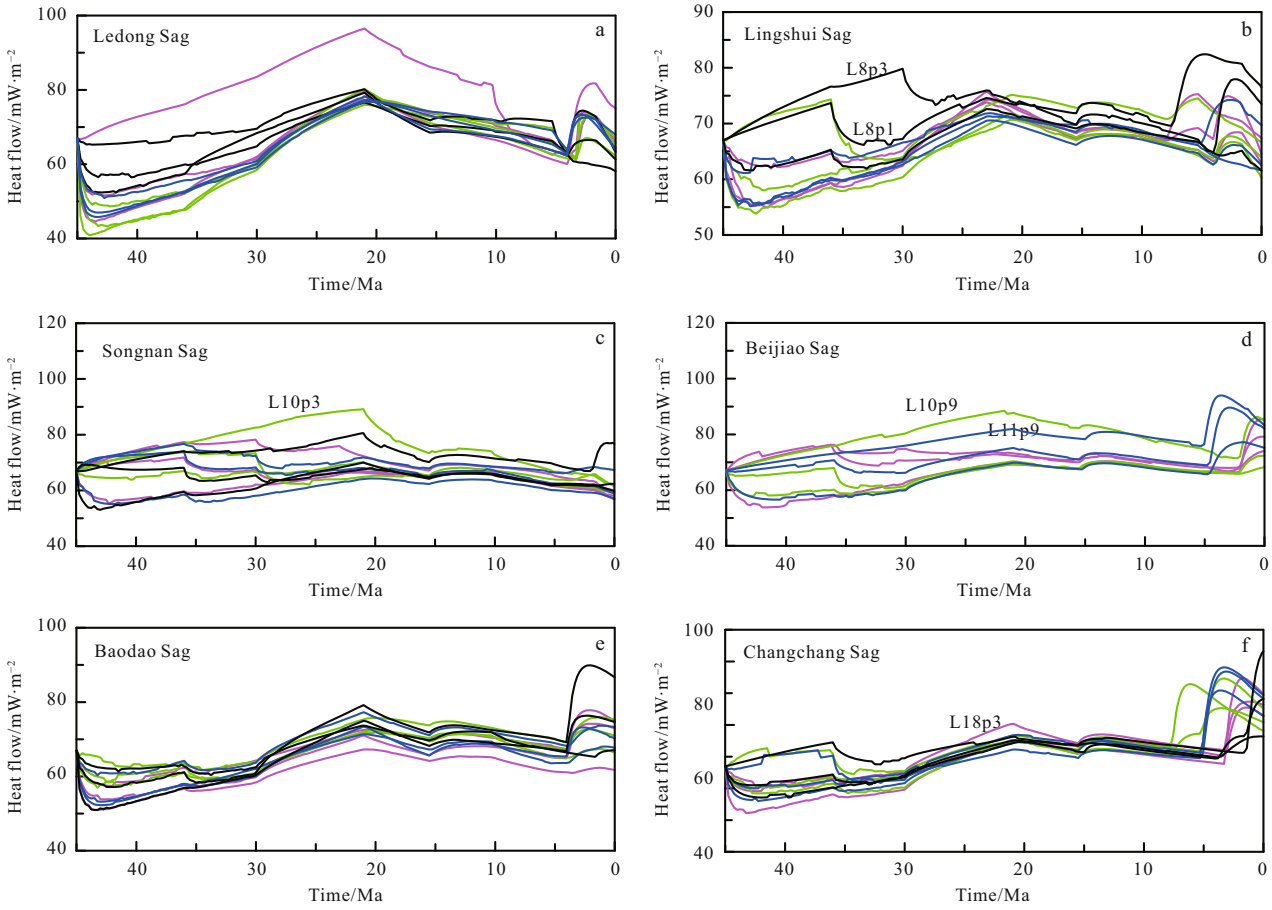

Fig.8. Heat flow histories of the representative points in the deep-water sags. The locations of the points are given in Fig. 2. The red, green, blue and black curves are the heat flow histories of the points along the profiles from west to east in each sag, respectively. L1p3 delegates the third point from north to south along Pm01. The present time is 0 Ma.

surface heat flow increased generally with time, and was higher in the basement high area, such as the northern uplift zone, and the Lingnan low basement high, the Songnan low basement high, and the southern uplift zone, than in their adjacent sags due to thermal refraction and thermal blanketing. Figure 9 is the surface heat flow distribution of the Qiongdongnan Basin at the end of the syn-rift phase. It shows that the heat flow in the Lingnan low basement high, the Songnan low basement high, and the southern rise zone was in a range of 75–100 mW/m^2, the heat flow in the northern rise zone was also higher than that in its adjacent sags. The heat flow was about 70–80 mW/m^2 in the Ledong sag, 70–75 mW/m^2 in the Lingshui sag, 60–75 mW/m^2 in the Songnan sag and the Beijiao sag. The heat flow in the Baodao and Changchang sags increased generally eastward in a range of 65–85 mW/m^2.

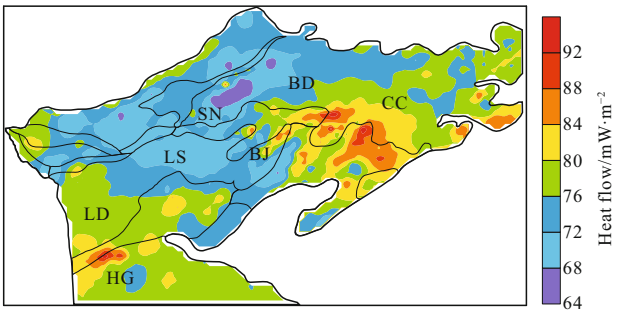

Fig.9. Predicted heat flow in the Qiongdongnan Basin at 21 Ma.

During the post-rift phase, with the sedimentary cover getting thicker in the basement highs, and the cooling of the lithosphere, the heat flow values and their difference in both the basement high and the sags decreased gradually (Figs 6–8). Figure 10 is the surface heat flow distribution of the Qiongdongnan Basin at around 10.5 Ma. It shows that heat flow in the central depression zone, Lingnan low high and the northern rise zone was in a range of 64–76 mW/m^2. In the Changchang sag, the eastern Songnan low basement high, and the southern uplift zone, due to the low deposition rate and thin sedimentary cover, the thermal blanketing was not strong enough to decrease greatly the heat flow. Therefore, the heat flow in these areas was still higher than 70 mW/m^2. Particularly in the Songnan low basement high and the eastern southern uplift zone, the heat flow was in a range of 75–85 mW/m^2.

However, due to the equivalent thermal events taking place at around 5 Ma, the heat flow in the central depression zone and the southern uplift zone increased again. The thermal events might be related to the widespread magmatism during the late post-rift phase. However, because of the rapid cooling of volcanic intrusion (Nissen et al., 1995; Shi et al., 2005), only the basaltic thermal events intruding at around 5 Ma or younger might have obvious effect on the present thermal field. If the numerical model did not include the thermal event, the predicted present heat flow would be 10–25 mW/m^2 lower than the observed heat flow in the central depression zone and the southern uplift zone (Figs 6 and 7). Figure 11 is the present heat flow contribution of the equivalent thermal event. It shows that the effect of the thermal event focuses obviously on the central depression zone and the southern uplift zone. The contribution in the western central depression zone and the Lingnan low high is generally lower than 15 mW/m^2, while it could be up to 25 mW/m^2 in the Songnan low high and the Baodao–Changchang sags, suggesting obviously that the thermal event contributes much more heat flow in the east than in the west (Figs 6, 7 and 11). Figure 11 also shows that the contribution of the thermal event is limited or negligible in the northern depression zone and the northern uplift zone. As a result, it becomes much hotter in the central depression zone and the southern uplift zone than in the northern depression and uplift zones, thus heat flow in most of the central depression zone is now higher than 70 mW/m^2 with an eastward increasing trend, and there is a NE trending high heat flow zone of 85–105 mW/m^2 lying in the eastern basin (Fig. 2).

5 Influence factors on the geothermal features of the deep-water area

Highly stretching of the lithosphere might be partly responsible for the high heat flow feature in the deep-water area. A heat flow map shows that the heat flow increases from the northern shelf (<70 mW/m^2) to the deep-water central depression zone and southern uplift zone (>65 mW/m^2) (Fig. 2). In the deep-water area, heat flow generally increases eastward and develops a high heat flow zone (>85 mW/m^2) in the Songnan basement low high, the Baodao sag, the Changchang sag and the northern slope of the Xisha Trough. On the basis of the gravity and seismic data, the crust in the central depression zone and the Xisha Trough is generally thinner than 15 km (e.g., Su et al., 2004; Qiu et al., 2001; Huang et al., 2011; Zhang et al., 2007; Zhang et al., 2009), particularly, the crust might be thinner than 10 km in the Xisha Trough and the Ledong sag. It indicates that the lithosphere in these areas has been highly stretched and thinned. Since the duration of the post-rift phase is about 21 Ma, which is not enough to recover the thermal balance, the highly rifting of the lithosphere might still contribute to part of the high heat flow in the deep-water area (McKenzie, 1978).

Another important factor might be the recent thermal event caused by the widespread magmatism. Since the cessation of the seafloor spreading of the South China Sea at around 16 Ma, basaltic magmatism activities have become much widespread and active, especially in South China (e.g., northern Hainan Island, Leizhou Peninsula, Beibu Gulf Basin), Indo-China (e.g., southern Thailand, southern Vietnam, southern Laos, southeastern Cambodia) and the South China Sea. The age histogram of the Cenozoic volcanism in these areas (Xu et al., 2012) indicates that a great amount of igneous activities have occurred since the Pliocene in the South China Sea and its adjacent regions. In the Xisha Trough and Qiongdongnan Basin, numerous magmatic injections have been identified based on seismic reflection profiles, magnetic data, seafloor geomorphologic map and drill samples, suggesting that extensive magmatic activities might have occurred during the late post-rift phase. For example, a tholeiitic basalt layer of around 115 m in thickness was found in the Pliocene of Drill Y32-1-1, offshore the SW Hainan Island (Li et al., 1998). Profile Pm20 shows some injections in its southern part (Fig. 5). In Fig. 1, there is a big intrusion body just exposed in the joint area between the Baodao sag and Changchang sag. However, though extensive magmatism might have affected the thermal regime of the study area, since an intrusion's thermal effect dissipates very quickly (Shi et al., 2005), the magmatism earlier than 5 Ma thus could have little effect on the present thermal regime. The above numerical analyses show that the relict heat caused by the thermal event equivalently occurred at around 5 Ma, could still contribute 10–25 mW/m^2 to the present surface heat flow in the deep-water area. Therefore, the observed high heat flow in the central depression zone, particularly in the high heat flow zone of the eastern basin, might be closely related to the magmatism since the Late Miocene.

The high heat flow in the deep-water area of the study area might also partly attribute to the thermal anomaly in the upper mantle. The geophysical and geochemical data show that the upper mantle below the Hainan Island is thermally anomalous. Regional and global tomographic studies suggested that there was a NW–SE dipping low velocity zone clearly beneath the

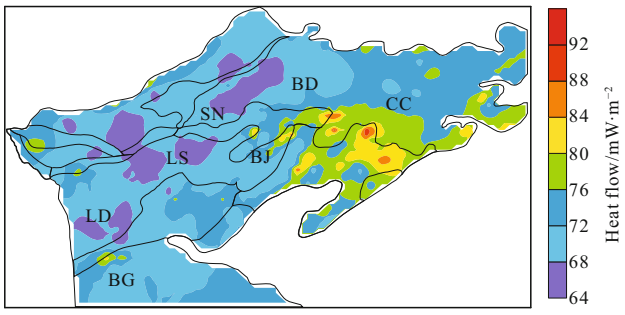

Fig.10. Predicted heat flow in the Qiongdongnan Basin at 10.5 Ma.

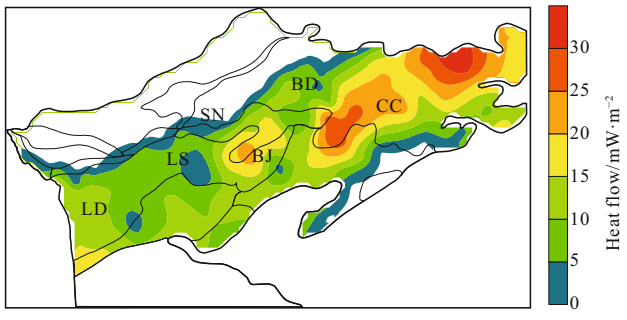

Fig.11. Predicted heat flow contribution of the recent thermal event.

Hainan Island (e.g., Lei et al., 2009; Lebedev and Nolet, 2003), which was thought to be the appearance of the Hainan plume (Zhao, 2007; Yan and Shi, 2007). Geochemical and petrological evidences such as the existence of extensive synchronous OIB-type basalts, high mantle potential temperature and geochemical signatures of the basalts from a lower mantle plume (e.g., Wang et al., 2013), suggest that the extensive magmatism in the South China Sea and its adjacent area since the Miocene was related to the deep anomalous thermal source. Therefore, the thermal anomaly in the upper mantle affects the thermal regime not only by providing deep heat source, but also by magmatism. The high heat flow in the deep-water Qiongdongnan Basin and the Xisha Trough might be the combined effects of the thermal anomaly in the upper mantle, highly stretched lithosphere, and recent widespread magmatism.

Besides the above important factors, there are some secondary factors which might have affected the heat flow distribution in the study area. These factors include basement and seafloor topography, sediment heat generation, sedimentary thermal blanketing, local injection body, hydrothermal activities related to faulting and overpressure. In the central depression zone, the Cenozoic is about 15 km in thickness in the western basin, while it is about 4 km in the easternmost basin and the Xisha Trough. If assuming an average heat production rate 1.34 μW/m^{3}①, the Cenozoic in the Ledong sag would contribute more than 15 mW/m^2, while in the Xisha Trough, it would generate about 5 mW/m^2. Since the thermal conductivity of the basement rock is generally higher than that of the sedimentary rock, heat tends to flow more to the basement high area, which is called thermal refraction effect. As a result, if the sediment cover is much thinner in the basement high area than that in its adjacent sags, the surface heat flow in the basement high area would be higher than that in the adjacent sags. The tectonic thermal analyses (Figs 6 and 7) show that during the syn-rift phase, the heat flow in the basement highs generally higher than that in the adjacent sags is the results of the thermal refraction effect. If the above numerical model does not consider the sedimentary thermal effect, it would generate a misleading heat flow distribution and the predicted heat flow in the central sag would be much higher than that in the adjacent basement highs. With the basement high covered with thicker and thicker sediment, the heat flow would redistribute and the heat flow difference would get smaller and smaller between these adjacent tectonic units. The present high heat flow in the southern uplift zone might partly attribute to the thin Cenozoic cover, which makes the increased heat flow due to the thermal refraction in deep not yet totally redistributed. The seafloor topography also has an effect on the heat flow distribution. In the shallow water area, higher thermal

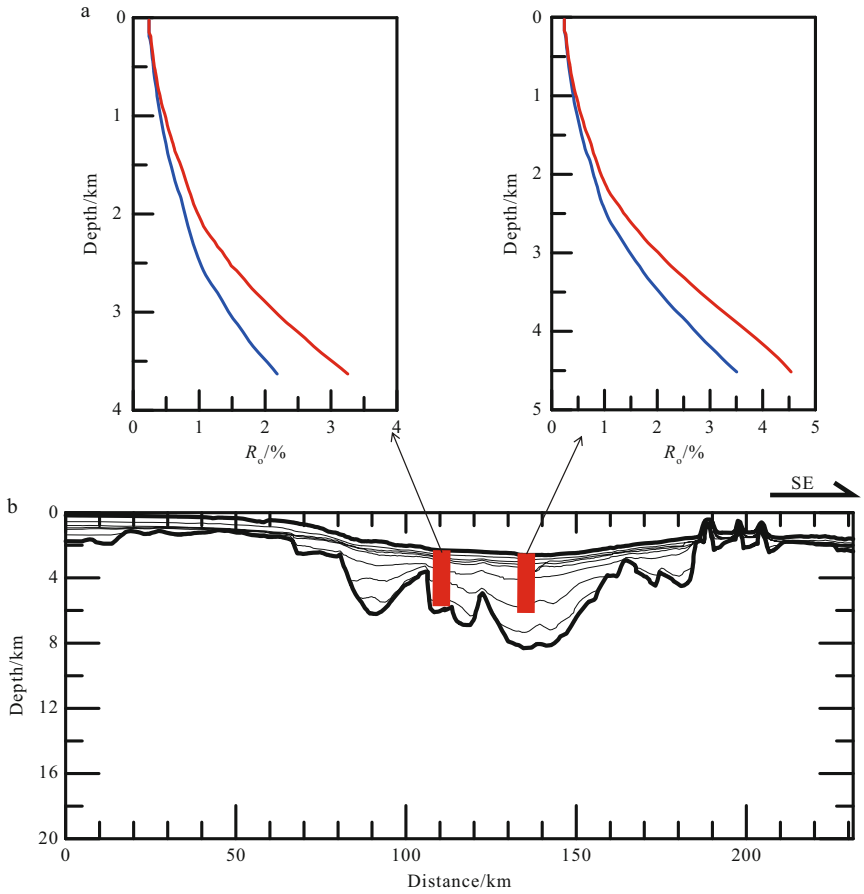

Fig.12. Effect of the recent thermal event on R_o data along Pm20. a. The predicted R_o data of two assumed drills. The blue lines show the R_o data without the effect of the thermal event, while the red lines show the data affected by the thermal event. b. The red lines show the locations of the two assumed drills on Profile Pm20.

resistance due to higher seafloor topography makes heat run to the adjacent deep-water area. Therefore, besides the difference in the thermal background and the effect degree of the recent thermal event, the difference in seafloor topography might be one factor partly responsible for the shelf's lower heat flow. The sedimentary thermal blanketing could decrease the surface heat flow. How much it would decrease the heat flow value mainly depends on sediment thermophysical property, deposition rate and the sedimentation duration. The higher the recent deposition rate, the larger the heat flow would be decreased. Hot basaltic intrusion would increase the local heat flow, and the spatial extension and the temporal duration it would affect depend on its scale. Generally an intrusion earlier than 5 Ma might have little effect on the present heat flow. Hydrothermal activities due to local faulting and overpressure also can cause the local heat flow anomaly, particularly in the western Qiongdongnan Basin where the overpressure is well developed. It is worth to say, except for local injection body and hydrothermal activities, all the other factors have been considered in our numerical model.

The recent thermal event would induce the further maturity of the source rock. Figure 12 compares the predicted R_o data whether there is the thermal event or not. It shows that the recent thermal event could have further induced the organic maturity. It is significant for the source rock in the eastern basin where the sediment thickness is much thinner than that in the western basin. Owing to the thin sediment, the lower-level thermal evolution of the source rock might be not enough to completely transform into hydrocarbon if there was no thermal event. Therefore, the recent thermal event might be beneficial for a hydrocarbon exploration in the eastern deep-water basin.

6 Conclusions

(1) On the basis of the present heat flow data, the Qiongdongnan Basin could be divided into three regions: the northern shelf and upper slope region with a heat flow of 50–70 mW/m^2, most of the central depression zone of 70–85 mW/m^2, and a NE trending high heat flow zone of 85–105 mW/m^2 lying in the eastern basin.

(2) The numerical results show that during the syn-rift phase, the heat flow increased generally with time, and was higher in the basement high area than in its adjacent sags. At the end of the syn-rift phase, the heat flow in the deep-water area was 65–85 mW/m^2, and the heat flow in the basement highs was 75–100 mW/m^2. During the post-rift phase, the heat flow decreased gradually, and tended to be more uniform in the adjacent tectonic units. However, extensive magmatism, which equivalently happened at around 5 Ma, increased the heat flow greatly, and still contributes about 10–25 mW/m^2 to the present surface heat flow in the central depression zone and the southern uplift zone.

(3) The high heat flow feature in the deep-water area is a combined results of the thermal anomaly in the upper mantle, highly thinning of the lithosphere and recent extensive magmatism. Other secondary factors might also have affected the heat flow distribution features in some local regions. These factors include basement and seafloor topography, sediment heat generation, thermal blanketing, local magmatic intrusion and hydrothermal activities related to faulting and overpressure.

Acknowledgements

Figures 1, 2 and 3 were plotted using GMT (Wessel and Smith, 1995). The geothermal features of the deep-water area were mostly based on the heat flow data of Xu Xing from the Guangzhou Marine Geological Survey Bureau.

References

Gong Zaisheng, Li Sitian, Xie Taijun, et al. 1997. Continental Margin Basin Analysis and Hydrocarbon Accumulation of the Northern South China Sea. Beijing: Science Press, 1–178

He Liansheng, Wang Guangyu, Shi Xiaochao. 1980. Xisha Trough—a Cenozoic rift. Geological Revolution (in Chinese), 26(6): 486–489

He Lijuan, Wang Kelin, Xiong Liangping, et al. 2001. Heat flow and thermal history of the South China Sea. Physics of the Earth and Planetary Interiors, 126: 211–220

Huang Haibo, Qiu Xuelin, Xu Huilong, et al. 2011. Preliminary results of the earthquake observation and the onshore-offshore seismic experiments on Xisha block. Chinese Journal of Geophysics, 54: 3161–3170

Lebedev S, Nolet G. 2003. Upper mantle beneath Southeast Asia from S velocity tomography. J Geophys Res, 108: 20–48

Lei Jianshe, Zhao Dapeng, Steinberger B, et al. 2009. New seismic constraintson the upper mantle structure of the Hainan plume. Phys Earth Planet Inter, 173(1): 33–50

Li Sitian, Lin Changsong, Zhang Qiming, et al. 1998. Episodic rifting dynamic of marginal basins north of South China Sea and tectonic accidents since 10 Ma. Chinese Science Bulletin (in Chinese), 43(8): 797–810

Li Yamin, Shi Xiaobin, Xu Huilong, et al. 2011. Analysis on activity characteristics of the Paleogene basement faults in Qiongdongnan Basin. Journal of Tropical Oceanogaphy (in Chinese), 30(6): 74–83

Li Xuxuan, Zhu Guangxu. 2005. The fault system and its hydrocarbon carrier significance in Qiongdongnan basin. China Offshore Oil and Gas (in Chinese), 17(1): 1–7

McKenzie D. 1978. Some remarks on the development of sedimentary basins. Earth and Planetary Science Letters, 40: 24–32

Mi Lijun, Yuan Yusong, Zhang G C, et al. 2009. Charateristics and genesis of geothermal field in deep-water area of the northern South China Sea. Acta Petrolei Sinica (in Chinese), 30(1): 27–32

Montelli R, Nolet G, Dahlen F A, et al. 2006. A catalogue of deep mantle plumes: new results from finite frequency tomography. Geochem Geophys Geosys, 7(11): doi: 10.1029/2006GC001248

Nissen S S, Hayes D E, Yao B. 1995. Gravity heat flow, and seismic constrints on the processes of crustal extension: Northern margin of the South China Sea. Journal of Geophysical Research, 100(B11): 22447–22483

Pang Xiong, Shen Jun, Yuan Lizhong, et al. 2006. Petroleum prospect in deep-water fan system of the Pearl River in the South China Sea. Acta Petrolei Sinica (in Chinese), 27(3): 11–16, 21

Qin Jingxin, Hao Tianyao, Xu Ya, et al. 2011. The distribution characteristics and the relationship between the tectonic units of the Moho depth in South China Sea and adjacent areas. Chinese J Geophys (in Chinese), 54(12): 3171–3183

Qiu Xuelin, Ye Sanyu, Wu Shimin, et al. 2001. Crustal structure across the Xisha Trough, northwestern South China Sea. Tectonophysics, 341(1–4): 179–193

Rupke L H, Schmalholz S M, Schmid D W, et al. 2008. Automated thermotectonostratigraphic basin reconstruction: Viking Graben case study. Aapg Bulletin, 92: 309–326

Shan Jingnan, Zhang Gongcheng, Wu Jingfu, et al. 2011.Thermal structure and deep temperature of Qiongdongnan Basin, Northern Margin of the South China Sea. Chinese J Geophys (in Chinese), 54(8): 2102–2109

Shi Xiaobin, Burov E, Leroy S, et al. 2005. Intrusion and its implication for subsidence: a case from the Baiyun Sag, on the northern margin of the South China Sea. Tectonophysics, 407: 117–134

Shi Xiaobin, Qiu Xuelin, Xia Kanyuan, et al. 2003. Characteristics of the

surface heat flow in the South China Sea. Journal of Asian Earth Sciences, 22(3): 265–277

Shi Xiaobin, Xu Hehua, Qiu Xuelin, et al. 2008. Numerical modeling on the relationship between thermal uplift and subsequent rapid subsidence: Discussions on the evolution of the Tainan Basin. Tectonics, 27(6): TC6003, doi: 10.1029/2007TC002163

Song Yang, Zhang Changyu, Zhang Gongcheng, et al. 2011. Research on tectono-thermal modeling for Qiongdongnan Basin and Pearl River Mouth Basin in the northern South China Sea. Chinese J Geophys (in Chinese), 54(12): 3057–3069

Su Daquan, Liu Yuanlong, Chen Xue, et al. 2004. 3D Moho depth of the South China Sea. In: Zhang Zhongjie, Gao Rui, Lv Qingtian, et al., eds. Earth's Deep Structure and Dynamic Researches of the Mainland China (in Chinese). Beijing: Science Press, 357–365

Tang Qunshu, Zheng Chan. 2013. Crust and upper mantle structure and its tectonic implications in the South China Sea and adjacent regions. Journal of Asian Earth Sciences, 62(2013): 510–525

Wang Xuance, Li Zhengxiang, Li Xianhua, et al. 2013. Identification of an ancient mantle reservoir and young recycled materials in the source region of a young mantle plume: Implications for potential linkages between plume and plate tectonics. Earth and Planetary Science Letters, 377: 248–259

Wang Zhengfeng, Li Xushen, Sun Zhipeng, et al. 2011. Hydrocarbon accumulation conditions and exploration potential in the deep-water region, Qiongdongnan basin. China Offshore Oil and Gas (in Chinese), 23(1): 7–13

Wessel P, Smith W H F. 1995. New version of the generic mapping tools. Eos, Transactions American Geophysical Union, 76(33): 329–329

White N, Thompson M, Barwise T. 2003. Understanding the thermal evolution of deep-water continental margins. Nature, 426: 334–343

Xie Wenyan, Zhang Yiwei, Sun Zhen, et al. 2007. Characteristics and formation mechanism of faults in Qiongdongnan basin. Marine Geology & Quaternary Geology (in Chinese), 27(1): 71–78

Xu Xing, Shi Xiaobin, Luo Xianhu, et al. 2006. Heat flow measurements in the Xisha trough of the South Chinas Sea. Marine Geology & Quaternary Geology (in Chinese), 26(4): 51–58

Xu Yigang, Wei Jingxian, Qiu Huaning, et al. 2012. Opening and evolution of the South China Sea constrained by studies on volcanic rocks: Preliminary results and a research design. Chinese Science Bulletin, 57(20): 3150–3164

Yan Quanshu, Shi Xuefa. 2007. Hainan mantle plume and the formation and evolution of the South China Sea. Geological Journal of China Universities (in Chinese), 13: 311–322

Yao Bochu, Zeng Weijun, Hayes D E, et al. 1994. The Geological Memoir of South China Sea Surveyed Jointly by China & USA (in Chinese). Wuhan: China University of Geosciences Press, 34–140

Yuan Yusong, Zhu Weilin, Mi Lijun, et al. 2009. "Uniform geothermal gradient" and heat flow in the Qiongdongnan and Pearl River Mouth Basins of the South China Sea. Marine and Petroleum Geology, 26: 1152–1162

Zhang Zhongjie, Liu Yifei, Zhang Sufang, et al. 2009. Crustal P wave velocity structure and layering beneath Zhujiangkou–Qiongdongnan Basins in the northern continental margin of South China Sea. Chinese Journal of Geophysics (in Chinese), 52(10): 2461–2471

Zhang Yunfan, Sun Zhen, Zhou Di, et al. 2007. The crust thinning characteristics and its dynamics meaning of northern margin of South China Sea. Science in China (Series D), 37(12): 1609–1616

Zhang Jian, Wang Jiyang. 2000. The deep thermal characteristic of continental margin of the northern South China Sea. Chinese Science Bulletin (in Chinese), 45(10): 1095–1100

Zhang Gongcheng, Zhu Weilin, Mi Lijun, et al. 2010. The theory of hydrocarbon generation controlled by source rock and heat from circle distribution of outside-oil fields and inside-gas fields in South China Sea. Acta Sedi Mentologica Sinica (in Chinese), 28(5): 987–1005

Zhao Dapeng. 2007. Seismic images under 60 hotspots: search for mantle plumes. Gondwana Res, 12: 335–355

Zhong Zhihong, Wang Liangshu, Li Xuxuan, et al. 2004. The paleogene basin-filling evolution of Qiongdongnan basin and its relation with seafloor spreading of the South China Sea. Marine Geology & Quaternary Geology (in Chinese), 24(1): 29–36

Zhu Weiling, Zhang Gongcheng, Yang Shaokun, et al. 2007. The Natural Gas Geology in Continental Margin Basin of the Northern South China Sea. Beijing: Petroleum Industry Press, 43–59